PAPER

Electrical and optical properties of InP nanowire ensemble p$^+$–i–n$^+$ photodetectors

To cite this article: Håkan Pettersson *et al* 2012 *Nanotechnology* **23** 135201
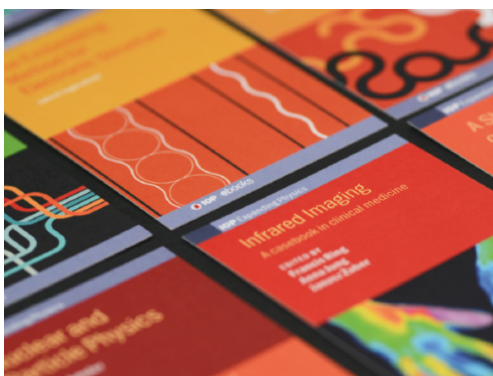
View the article online for updates and enhancements.

Electrical and optical properties of InP nanowire ensemble p$^+$–i–n$^+$ photodetectors

Håkan Pettersson[1,2], Irina Zubritskaya[1], Ngo Tuan Nghia[1], Jesper Wallentin[2], Magnus T Borgström[2], Kristian Storm[2], Lars Landin[1], Peter Wickert[3], Federico Capasso[4] and Lars Samuelson[2]

[1] Laboratory of Mathematics, Physics and Electrical Engineering, Halmstad University, Box 823, SE-30118 Halmstad, Sweden
[2] Solid State Physics and the Nanometer Structure Consortium, Lund University, Box 118, SE-22100 Lund, Sweden
[3] Sol Voltaics AB, Ideon Science Park, Scheelevägen 17, SE-22370 Lund, Sweden
[4] School of Engineering and Applied Sciences, Harvard University, Cambridge, MA 02138, USA

E-mail: hakan.pettersson@hh.se

Abstract
We report on a comprehensive study of electrical and optical properties of efficient near-infrared p$^+$–i–n$^+$ photodetectors based on large ensembles of self-assembled, vertically aligned i–n$^+$ InP nanowires monolithically grown on a common p$^+$ InP substrate without any buffer layer. The nanowires have a polytype modulated crystal structure of wurtzite and zinc blende. The electrical data display excellent rectifying behavior with an ideality factor of about 2.5 at 300 K. The ideality factor scales with $1/T$, which possibly reflects deviations from classical transport models due to the mixed crystal phase of the nanowires. The observed dark leakage current is of the order of merely ∼100 fA/nanowire at 1 V reverse bias. The detectors display a linear increase of the photocurrent with reverse bias up to about 10 pA/nanowire at 5 V. From spectrally resolved measurements, we conclude that the photocurrent is primarily generated by funneling photogenerated carriers from the substrate into the NWs. Contributions from direct excitation of the NWs become increasingly important at low temperatures. The photocurrent decreases with temperature with an activation energy of about 50 meV, which we discuss in terms of a temperature-dependent diffusion length in the substrate and perturbed transport through the mixed-phase nanowires.

(Some figures may appear in colour only in the online journal)

1. Introduction

Self-assembled nanowires (NWs) have for the past few years attracted considerable attention due to the interesting fundamental properties of such low-dimensional systems and the exciting prospects for utilizing these materials in future nanotechnology-enabled electronic and photonic applications [1]. For example, nanoscale field-effect transistors [2–4], inverters [3, 4] and more complex logic gates [4] have been demonstrated using well-defined NW building blocks. It is possible to form heterostructures in NWs [5–7] facilitating 1D electronics, e.g. resonant tunneling diodes [8], single-electron transistors [9] and field-effect transistors [10]. For photonic applications, LEDs [2], lasers [11] and photodetectors [12, 13] have also been assembled using NWs. Due to the small footprint of NWs, nanophotonic devices can be grown directly on silicon substrates where lattice mismatch of the NWs and silicon are accommodated by the NWs [14, 15] of

profound importance for realizing 'More than Moore'[5]. Large-area photodetectors based on monolithic integration of InAs NWs on silicon for efficient broad band photodetection was recently reported by Wei *et al* [16]. A complicating factor for these heterostructure devices is the band offset between the NWs and substrate. In order to increase the understanding of electronic properties of monolithic NW-based optoelectronics, it is therefore of interest to study devices fabricated from the same material.

Here we present a detailed study of electrical and optical properties of p^+–i–n^+ photodetectors based on ensembles of i–n^+ InP NWs vertically grown on an InP p^+ substrate, i.e. the substrate acts as a common p^+ contact to all the NWs. In contrast to NW-based p–i–n detectors with p-type segments integrated into the wires, our detector design in particular allows us to compare the efficiency of collecting photogenerated carriers from the substrate into the NWs to direct optical excitation of the NWs.

2. Experimental details

Samples were prepared for NW growth by depositing 80 nm Au particles in a density of 2.6, 0.69, 0.32 and 0.15 NWs μm^{-2} (observed and counted by SEM) on p^+-InP (111)B substrates (Zn-doped 5×10^{18} cm^{-3}) by an aerosol technique [17]. The NWs were subsequently grown in a low-pressure (100 mbar) metal–organic vapor phase epitaxy (MOVPE) system (Aixtron 200/4) with a total flow of $13 \, l \, min^{-1}$ using hydrogen (H_2) as carrier gas. For InP growth, trimethylindium (TMI) and phosphine (PH_3) were used as precursors, with constant molar fractions of $\chi_{TMI} = 21.1 \times 10^{-6}$ and $\chi_{PH3} = 6.9 \times 10^{-3}$. Tetraethyltin (TESn) was used as n-type doping precursor [18] at a molar fraction of $\chi_{TESn} = 9.9 \times 10^{-6}$. Hydrogen chloride (HCl) at a molar fraction of $\chi_{HCl} = 4.0 \times 10^{-6}$ was used to control the radial growth [19]. The samples were first annealed at 550 °C for 10 min under a PH_3/H_2 gas mixture to desorb any surface oxides. The reactor was then cooled to 420 °C, at which growth was initiated by adding TMI to the flow. After a 15 s nucleation time, HCl was added and nominally intrinsic InP with an residual doping concentration of about 10^{15} cm^{-3} was grown for 5 min and 42 s. Subsequently, TESn was switched on to grow n-InP for 4 min with a nominal donor concentration of about 10^{19} cm^{-3}. Then growth was terminated and the sample cooled down in a PH_3/H_2 gas mixture. An SEM image of the as-grown InP NWs is shown in figure 1(a). From previous studies it is known that NWs grown under the present conditions contain a polytype mixture of two different crystal phases—wurtzite and zinc blende [18]. The processing of the detectors started by depositing 200 nm insulating SiO_2 on top of the as-grown samples. A resist was thereafter spun-cast to planarize the structures. The SiO_2 at the top part of the NWs was removed in an etching procedure to expose the NW tip, after which the remaining resist was removed. The samples were further

---

[5] 'More than Moore' implies new functionality added to conventional mainstream digital electronics beyond merely an increase in transistor density.
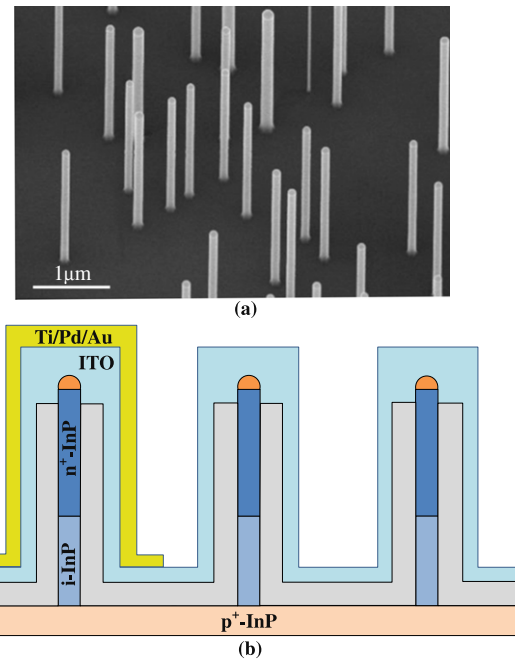
Figure 1. (a) SEM image of the as-grown InP NWs. (b) Schematic layout of the p^+–i–n^+ detector. Note that the NWs do not contain any p^+ segment. The Ti/Pd/Au contact is for bonding of the detector element.

processed using UV lithography to open up 1×1 mm^2 square detector windows, followed by sputtering of 300 nm ITO and lift-off. A second UV lithography step was subsequently carried out to open up smaller windows on the ITO squares for bond pad definition, followed by metallization and lift-off. As a final step, the samples were cleaned on the backside and mounted on DIL-14 chip carriers using the highly doped p-InP substrate as back contact. Figure 1(b) shows a schematic cross section of the device layout.

The spectrally resolved photocurrent (PC) was measured using a Bruker Vertex 80v Fourier transform spectrometer housing an integrated Oxford OptistatDN cryostat. The spectrometer was evacuated to avoid any influence of absorption lines in air. The spectrometer was equipped with a CaF_2 beamsplitter and a quartz lamp. The modulated (~5 kHz) PC was amplified using a Keithley 428 programmable current amplifier. The *IV* characteristics were taken with a Keithley 6430 sub-femtoampere source meter.

3. Results and discussion

We have carried out a comprehensive study of the electrical and optical properties of p^+–i–n^+ photodetectors with four different InP NW surface densities. In addition, we have investigated reference samples where the SiO_2 isolation layer, capping the NWs and substrate, was not back-etched prior to deposition of ITO. The current in these reference samples is negligible, indicating an excellent electrical quality of the oxide. Thus, any observed detector signals stem from transport through the NWs and not from spurious leakage currents through the oxide. Figure 2 shows the
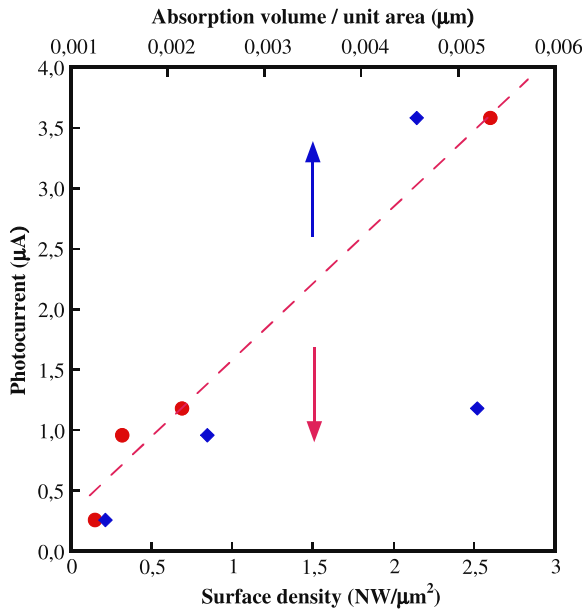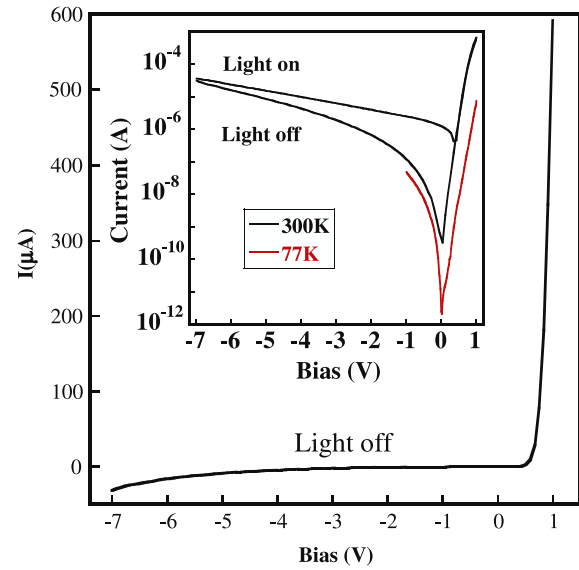
Figure 2. Integrated (all-wavelength) short-circuit current versus NW surface density (red points, lower panel) and absorption volume (blue points, upper panel). The dashed line is a linear fit to the red points.

Figure 3. *IV* characteristics in darkness at 300 K. Inset shows lin–log plot of the *IV* at 300 K (black curve) and 77 K (red curve), respectively. Note that the data shown under illumination also contains the dark current.

Figure 4. Dependence of dark (leakage) current on reverse bias at 300 K. Left panel shows integrated dark current and right panel the corresponding dark current per NW. The sample contains 690.000 NWs. Inset shows the data in a log–log plot.

integrated short-circuit (zero bias) photocurrent measured for detectors with different NW density (2.6, 0.69, 0.32 and 0.15 NWs μm^{-2}, respectively). While the diameter of the NWs is 80 nm for all samples, the length of the i-region varies (0.35, 1.5, 1.5 and 1.8 μm, respectively). We define the intrinsic absorption volume as the accumulated volume of the intrinsic regions from all NWs on a sample. From this data it is readily observed that the photocurrent scales quite well with the NW surface density (red color), rather than with the intrinsic absorption volume/unit area (blue color) of the NWs. We have also confirmed that the results displayed in figure 2 are valid if a reverse bias is applied to the samples. Already at this point we tentatively conclude that the main part of the photocurrent is most likely generated in the substrate and not directly in the i-region of the NWs. This conclusion is strengthened by the data presented in figures 5 and 6. The overall electrical and optical data of the different samples form a consistent picture that can be conveyed by presenting the detailed analysis of one NW density only. We have chosen to present the data for the detector with 0.69 NWs μm^{-2}. The reason for not choosing the detector with the highest surface density is that the length of the i-region in this case is only about 350 nm, as opposed to 1.5 μm for the present sample.

Figure 3 shows the *IV* characteristics in darkness and under illumination, respectively. From the slope of the $\log(I)$ versus *V* in the inset we deduce an ideality factor of about 2.5 at 300 K. Interestingly, the slope is relatively independent of temperature down to 77 K, implying an ideality factor $\sim \frac{1}{kT}$. Similar temperature-dependent ideality factors have previously been reported for disordered organic p–n junctions [20]. The deviation from classical transport models was attributed to violation of the Einstein relation ($\frac{qD}{\mu} = kT$) in the framework of diffusion theory [20]. In view
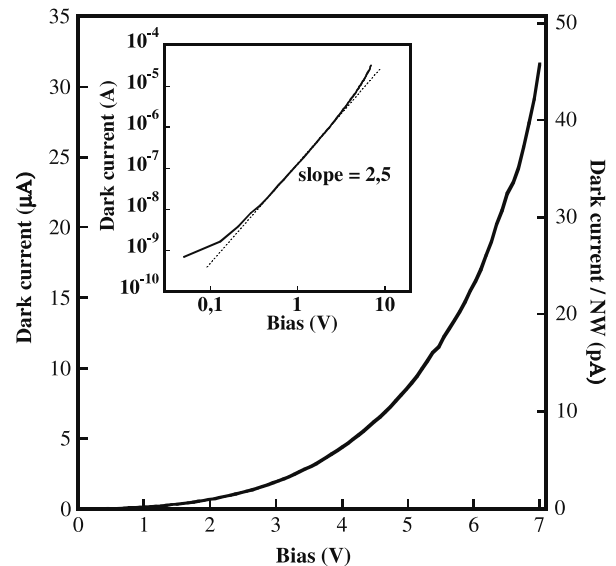
of the polytype structure of the NWs studied in the present work, similar arguments could explain our results. In the inset of figure 3, a clear photovoltaic effect is observed with an open-circuit voltage of about 0.70 V at 300 K, and integrated (all-wavelength) photocurrents in the microampere regime (corresponding to a few pA/NW).

In figure 3 it is also observed that the dark leakage current increases with reverse bias. Figure 4 shows this voltage dependence in more detail. At small bias, the leakage current is insignificant. At a reverse bias of about 1 V, the current amounts to an impressively low $\sim$100 fA/NW.
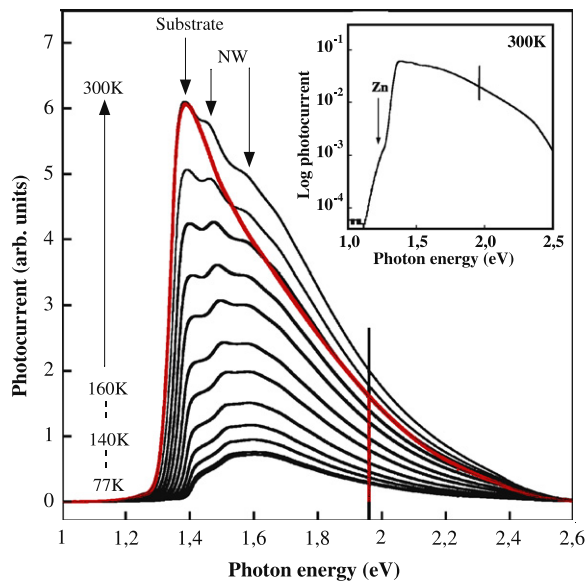
Figure 5. Spectrally resolved photocurrent at different temperatures. The sharp peak just below 2 eV is due to the internal reference laser in the spectrometer that keeps track of the scanning mirror. Inset shows log plot of photocurrent at 300 K. The red curve is a comparative spectrum recorded at 300 K for a different sample with highest surface density (2.6 NW μm^{-2}) and shortest i-segment (350 nm). It is normalized with respect to the 300 K spectrum of the main sequence. The spectra are not normalized with respect to the photon flux. Arrows indicate peaks related to interband transitions in the substrate and NWs, respectively.

We plot this data in a log–log format as the inset. From the slope we deduce an approximate quadratic dependence ($\sim V^{2.5}$) of the leakage current on reverse bias. The behavior is similar for the other samples, except for the high-density sample with short i-segment (350 nm) which displays a stronger ($\sim V^4$) bias dependence. At present, we do not have a clear understanding of the observed bias dependence. The leakage current increases with temperature for a constant reverse bias, implying a Zener tunneling mechanism. The length of the i-region, however, implies that the electric field is reduced and any conventional tunneling process should be strongly suppressed. The impact ionization mechanism is normally more important for p–i–n diodes. However, the temperature dependence should then be opposite to what is observed in our case. Also, avalanche processes typically display much more distinct breakdown characteristics at large bias. It should be mentioned that any breakdown mechanism could be different in nanoscale devices. It has, for example, been shown by detailed theoretical analysis that impact ionization can be significantly enhanced in nanostructures compared to bulk-form p–n junctions as a result of increased Coulomb interaction in confined nanostructures [21, 22]. The perhaps most plausible explanation is a bias-dependent surface leakage current. Nanoscale diodes are expected to suffer from strong surface leakage effects due to the large surface-to-volume ratio. It is worth noticing that surface leakage currents typically scale as $V^{0.5}$ or $V^{1/3}$, which is much weaker than observed in the present case. To unravel the detailed mechanism, more investigations are needed on
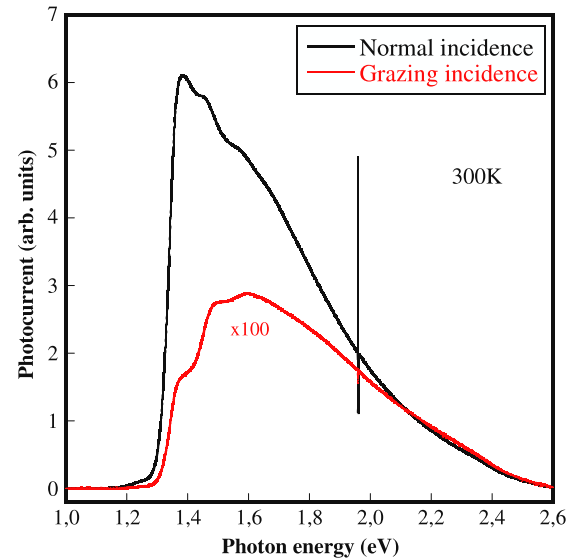
Figure 6. Spectrally resolved photocurrent for different angles of incoming radiation. The black spectrum is recorded at normal incidence (adopted from figure 5), while the red spectrum is taken under grazing incidence conditions (radiation nearly parallel to surface).

samples where both the length and diameter of the NWs are changed in a systematic way.

Figure 5 shows the spectrally resolved short-circuit current for the NW detector as a function of temperature. The position of the main peak (marked 'substrate') is in good agreement with the fundamental interband transition energy of bulk InP (confirmed by reference measurements on planar InP p–i–n diodes), and we attribute this peak to photoexcitation of the p$^+$ substrate. Interestingly, there is thus an effective funneling of photogenerated carriers from the substrate into the nanowires. It should be kept in mind that the penetration of the space–charge region at the foot of the NWs into the substrate is merely a few tens of nanometers given the nominal doping concentration. The two peaks marked 'NW' are attributed to photoexcitation of the NWs. As already mentioned, the NWs contain a mixture of two different crystal phases—wurtzite and zinc blende. Moreover, previous studies made on similar NWs indicate that the potential landscape along the wires is staggered (type II) with randomly alternating segments of wurtzite and zinc blende [23]. The bandgap of pure InP wurtzite is known to be at least 80 meV larger than for zinc blende [24], wherefore the NW peak at about 1.45 eV is attributed to fundamental interband excitation of the wurtzite segments. The second broader NW peak at about 1.60 eV can be attributed to the C-band in wurtzite InP, as previously observed in photoluminescence excitation spectroscopy (PLE) [25]. Any spectral signatures related to zinc blende segments, or to indirect transitions between wurtzite and zinc blende segments [23], are probably masked by the much stronger InP bulk signal. In figure 5, we plot for comparison the spectrally resolved photocurrent for a different sample with the highest surface density and shortest i-region (0.35 μm). The absence of NW-related peaks in this spectrum reflects the fact that the i-segment is too short to give

a noticeable contribution to the photocurrent and, hence, that photogenerated carriers in the substrate dominate the signal. In fact, by comparing this spectrum to the spectrum for the NW sample with the 1.5 μm i-region under investigation, the relative contribution from direct excitation of the NWs can be estimated to be about 15–20% at 300 K. Interestingly, it is readily observed that the contribution from direct excitation of the NWs increases strongly at lower temperatures, as evident from, for example, the 77 K spectrum where the signal from the substrate is drastically reduced. The inset of figure 5 shows the photocurrent at 300 K on a log scale. The shoulder below the bandgap of InP is attributed to optical transitions from zinc acceptors to the conduction band and from acceptors to deep donors [26] in the substrate. A further interesting observation in figure 5 is that no clear evidence of bandgap narrowing is observed in the highly doped substrate. An acceptor concentration of about 5×10^{18} cm^{-3} should induce a narrowing of about 50 meV [27]. A possible reason for this is that the subsequent growth of NWs leads to out-diffusion of Zn from the top layer of the substrate. A lower Zn concentration implies a larger penetration of the space–charge region into the substrate which would otherwise amount to only a few tens of nanometers.

We have also investigated the dependence of the spectral shape of the photocurrent on the angle of incidence of the radiation. In figure 6 we plot the spectrally resolved photocurrent at normal incidence and grazing incidence, respectively. Clearly, the substrate peak is strongly decreased at grazing incidence conditions when the incoming radiation is nearly parallel to the sample surface and primarily interacts with the NWs (compare the sample layout in figure 1(b)). The remaining substrate signal could, in fact, instead originate from excitation of the zinc blende segments in the NWs. We have also carried out polarization-dependent photocurrent measurements (not displayed) at grazing incidence. While the spectral shape is rather independent on polarization direction, the amplitude of the photocurrent roughly increases by a factor of 2 when the orientation of the electric field is rotated from being orthogonal to parallel with respect to the NWs.

Figure 7 shows the dependence of the integrated photocurrent on reverse bias at 300 K. The observed linear dependence is unexpected since the drift velocity in the i-region of p–i–n detectors is typically saturated already at low reverse bias. The inset of figure 7 shows the temperature dependence of the short-circuit current in the form of an Arrhenius plot. After subtracting the constant background signal, we deduce an activation energy of 54 meV. The calculated band offsets for the staggered zinc blende/wurtzite polytype NWs amount to 129 meV and 45 meV in the conduction band and valence band, respectively [28]. Since we do not have access to detailed TEM images of the as-grown NWs, we do not know the exact length and distribution of the different segments. For short zinc blende segments, a considerable confinement in the growth direction is expected and the activation energy we observe could then reflect the energy separation between the bound ground states of the zinc blende segments (quantum wells) and the wurtzite band edge leading to an effective temperature-activated transport
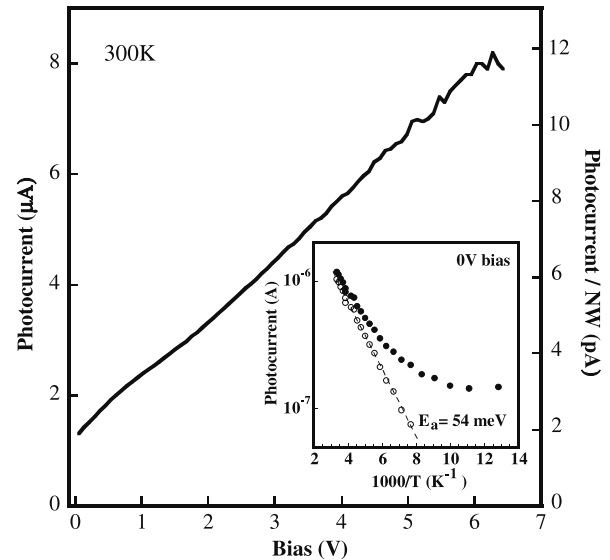
Figure 7. Dependence of integrated photocurrent on reverse bias at 300 K (dark current subtracted). Left panel shows integrated photocurrent from all NWs. Right panel shows the corresponding photocurrent per NW. Inset shows Arrhenius plot of short-circuit current (filled circles). Open circles are extracted by subtracting the constant low-temperature photocurrent. A fitting to these data points gives an activation energy of 54 meV.

of photogenerated carriers from the substrate through the NWs. There are, however, no clear traces of strongly confined zinc blende segments in the optical data, unless the interband transition energy of these segments coincides with the bandgap of the wurtzite segments. An alternative explanation of the temperature dependence of the photocurrent rather involves the temperature-dependent generation and transport mechanisms in the substrate itself. The diffusion length of photogenerated carriers in the highly doped substrate, given by $\sqrt{D\tau}$, is expected to display a superlinear T dependence $\sim \sqrt{TT^{1.5}}$ (assuming a defect-limited mobility and a classical Einstein relation). The corresponding diffusion current is proportional to the diffusion constant D. Moreover, the absorption coefficient for the interband transition is $\sim \sqrt{h\nu - E_g(T)}$. The decrease of the bandgap with increasing temperature leads to an enhanced photocurrent at elevated temperatures. Combining the temperature dependence of the generation and transport mechanisms would give a roughly quadratic dependence which can be confirmed by plotting the photocurrent versus temperature on a log–log plot (not shown), rather than in an Arrhenius format. The linear bias dependence in this model would reflect an enhanced collection of diffusing photogenerated carriers from the substrate into the NWs. More detailed studies of the photoresponse of single InP NW p–i–n detectors are needed to separate transport mechanisms related to the substrate and to the NWs, respectively.

4. Conclusions

In summary, we have presented a study of electrical and optical properties of near-infrared p$^+$–i–n$^+$ photodetectors

based on large ensembles of self-assembled InP NWs grown directly on InP substrates without a buffer layer. The samples display excellent rectifying behavior with an ideality factor of about 2.5 at 300 K and small leakage currents at low reverse bias ($\sim$100 fA/NW@1 V). From the optical data, we conclude that the photocurrent is primarily generated by funneling photogenerated carriers from the substrate into the NWs. Contributions from direct excitation of the NWs become increasingly important at low temperatures. The observed temperature and bias dependence of the photocurrent is discussed in terms of limiting transport mechanisms in the substrate and mixed-phase NWs.

Acknowledgments

References

[1] see e.g. Hu J, Odom T W and Lieber C M 1999 *Acc. Chem. Res.* **32** 435

[2] Duan X, Huang Y, Cui Y, Wang J and Lieber C M 2001 *Nature* **409** 66

[3] Cui Y and Lieber C M 2001 *Science* **291** 851

[4] Huang Y, Duan X, Cui Y, Lauhon L J, Kim K-H and Lieber C M 2001 *Science* **291** 630

[5] Björk M T, Ohlsson B J, Sass T, Persson A I, Thelander C, Magnusson M H, Deppert K, Wallenberg L R and Samuelson L 2002 *Appl. Phys. Lett.* **80** 1058

[6] Lieber C M, Gudiksen M S, Lauhon L J, Wang J and Smith D C 2002 *Nature* **415** 617

[7] Li D Y, Wu Y, Fan R, Yang P D and Majumdar A 2003 *Appl. Phys. Lett.* **83** 3186

[8] Björk M T, Ohlsson B J, Thelander C, Persson A I, Deppert K, Wallenberg L R and Samuelson L 2002 *Appl. Phys. Lett.* **81** 4458

[9] Thelander C, Mårtensson T, Björk M T, Ohlsson B J, Larsson M W, Wallenberg L R and Samuelson L 2003 *Appl. Phys. Lett.* **83** 2052

[10] De Franceschi S, van Dam J A, Bakkers E P A M, Feiner L F, Gurevich L and Kouwenhoven L P 2003 *Appl. Phys. Lett.* **83** 344

[11] Huang M H, Mao S, Feick H, Yan H, Wu Y, Kind H, Weber E, Russo R and Yang P 2001 *Science* **292** 1897–9

[12] Wang J, Gudiksen M S, Duan X, Cui Y and Lieber C M 2001 *Science* **293** 1455

[13] Pettersson H, Trägårdh J, Persson A I, Landin L, Hessman D and Samuelson L 2006 *Nano Lett.* **6** 229

[14] Svensson C P T, Mårtensson T, Trägårdh J, Larsson C, Rask M, Hessman D, Samuelson L and Ohlsson J 2008 *Nanotechnology* **19** 305201

[15] Mårtensson T, Borgström M, Seifert W, Ohlsson B J and Samuelson L 2003 *Nanotechnology* **14** 1255

[16] Wei W, Bao X-Y, Soci C, Ding Y, Wang Z-L and Wang D 2009 *Nano Lett.* **9** 2926

[17] Magnusson M H, Deppert K, Malm J O, Bovin J O and Samuelson L 1999 *Nanostruct. Mater.* **12** 45

[18] Borgström M T, Norberg E, Wickert P, Nilsson H A, Trägårdh J, Dick K A, Statkute G, Ramvall P, Deppert K and Samuelson L 2008 *Nanotechnology* **19** 445602

[19] Borgström M T, Wallentin J, Trägårdh J, Ramvall P, Ek M, Wallenberg L R, Samuelson L and Deppert K 2010 *Nano Res.* **3** 264

[20] Harada K, Werner A G, Pfeiffer M, Bloom C J, Elliott C M and Leo K 2005 *Phys. Rev. Lett.* **94** 036601

[21] Fu Y, Hellström S and Ågren H 2009 *J. Nonlinear Opt. Phys. Mater.* **18** 195

[22] Fu Y, Zhou Y-H, Su H, Boey F Y C and Ågren H 2010 *J. Phys. Chem.* C **114** 3743

[23] Bao J, Bell D C, Capasso F, Wagner J B, Mårtensson T, Trägårdh J and Samuelson L 2008 *Nano Lett.* **8** 836

[24] Mattila M, Hakkarainen T, Mulot M and Lipsanen H 2006 *Nanotechnology* **17** 1580

[25] Perera S, Pemasiri K, Fickenscher M A, Jackson H E, Smith L M, Yarrison-Rice J, Paiman S, Gao Q, Tan H H and Jagadish C 2010 *Appl. Phys. Lett.* **97** 023106

[26] Moon Y, Si S, Yoon E and Kim S J 1998 *J. Appl. Phys.* **83** 2261

[27] www.ioffe.rssi.ru/SVA/NSM/Semicond/InP/

[28] Murayama M and Nakayama T 1994 *Phys. Rev.* B **49** 4710